Supporting Information

Tuning selectivity in nickel oxide-catalyzed oxidative dehydrogenation of ethane through control over non-stoichiometric oxygen density

Xiaohui Zhao, Mariano D. Susman, Jeffrey D. Rimer, and Praveen Bollini**

Department of Chemical and Biomolecular Engineering
University of Houston, 4726 Calhoun Rd., Houston, TX 77204, USA

*Correspondence sent to: jrimer@central.uh.edu or ppbollini@uh.edu

Table of Contents

1. Material Characterization

1.1 As-synthesized NiO cubes, octahedra and trapezohedra. All three samples synthesized via molten salt routes show a single phase that matches with the NiO reference pattern. Each faceted NiO presumably exposes a single type of surface facet; NiO {100} for cubes, {311} for trapezohedra, and {111} for octahedra. The proposed surface terminations and surface coordination numbers are shown in Scheme S1.

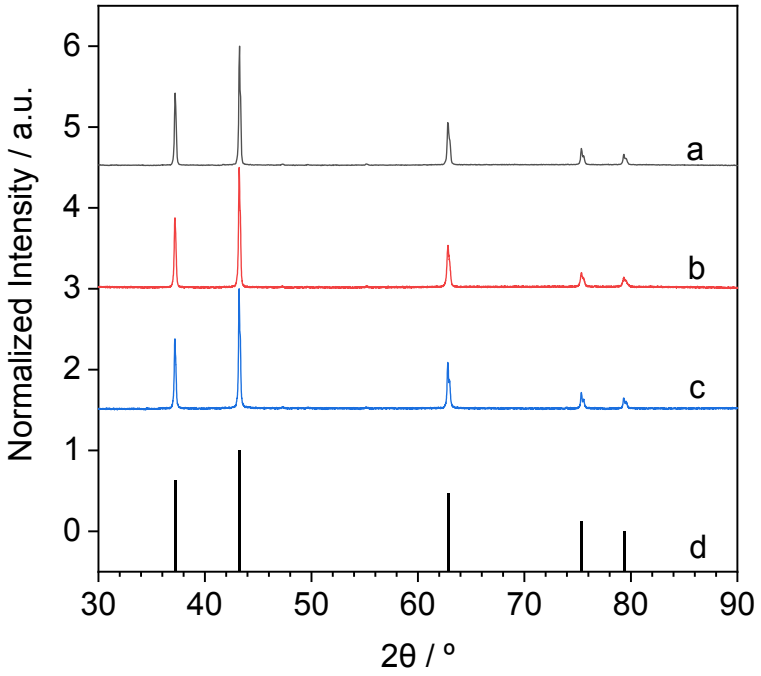

Fig. S1 Powder X-ray diffraction patterns of NiO (a) cubes, (b) octahedra, and (c) trapezohedra prepared by molten salt synthesis. (d) NiO reference pattern: ICSD-9866, cubic, *Fm-3m* (225).

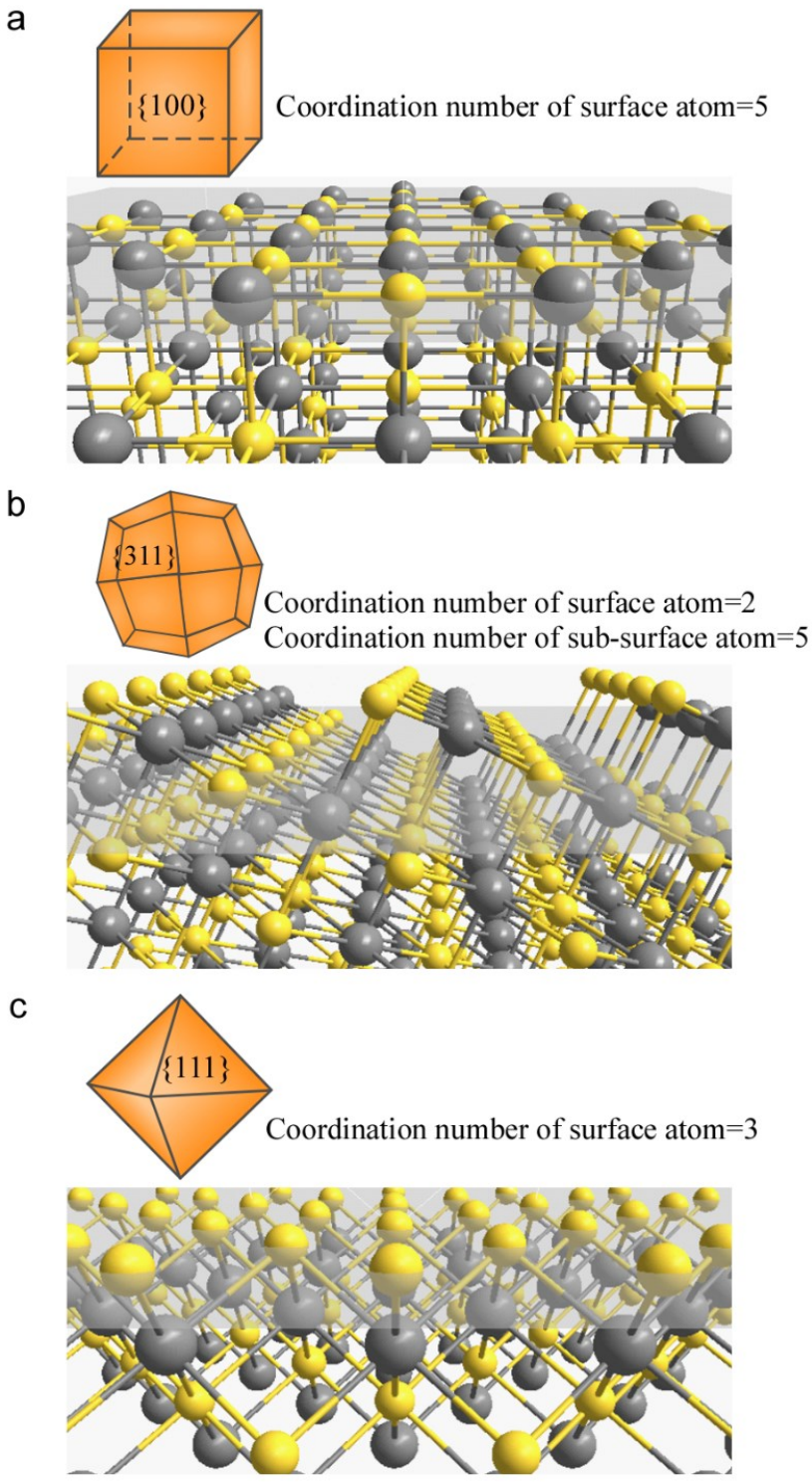

Scheme S1 Proposed surface structures of NiO (a) cubes exposing Ni/O-terminated {100} facets, (b) trapezohedra exposing O-terminated {311} facets, and (c) octahedra exposing O-terminated {111} facets. Crystal planes are indicated in light grey. Oxygen anions and nickel cations are indicated in yellow and grey spheres, respectively.

1.2 Thermally treated NiO cubes. PXRD patterns and SEM images show that NiO cubes were morphologically stable upon thermal treatments up to 1000 °C. Nitrogen physisorption isotherms suggest a loss in BET surface areas from 1.33 to 0.7 $m^2\ g^{-1}$ with increasing treatment temperature. The changing surface areas were taken into account when comparing areal rates.

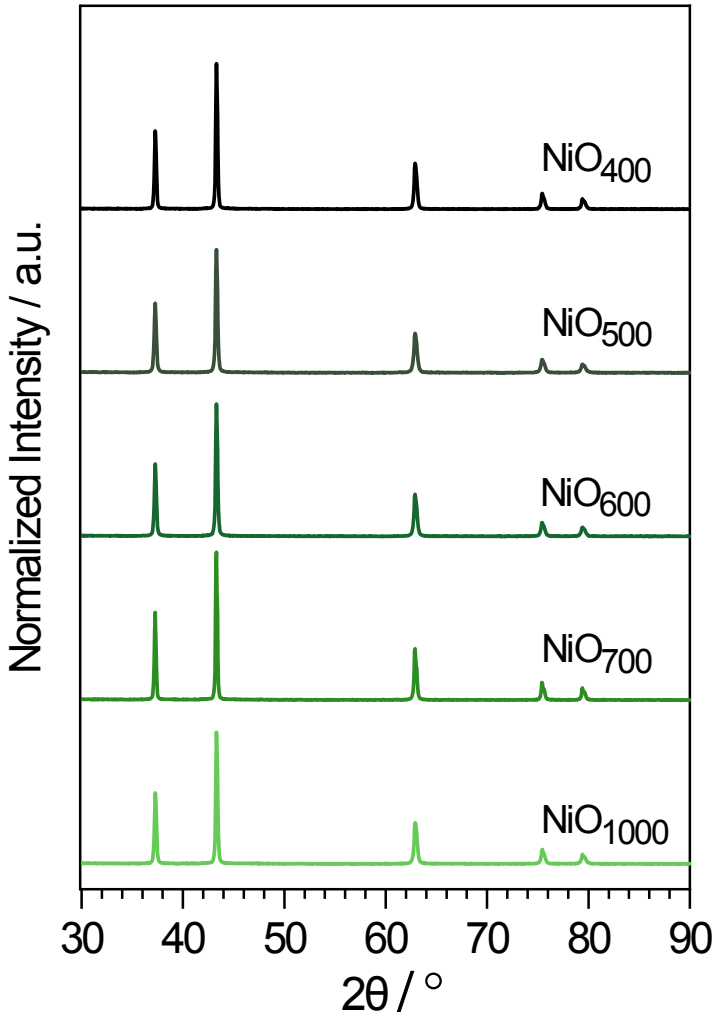

Fig. S2 Powder X-ray diffraction patterns of NiO samples treated at 400–1000 °C for 5 h.

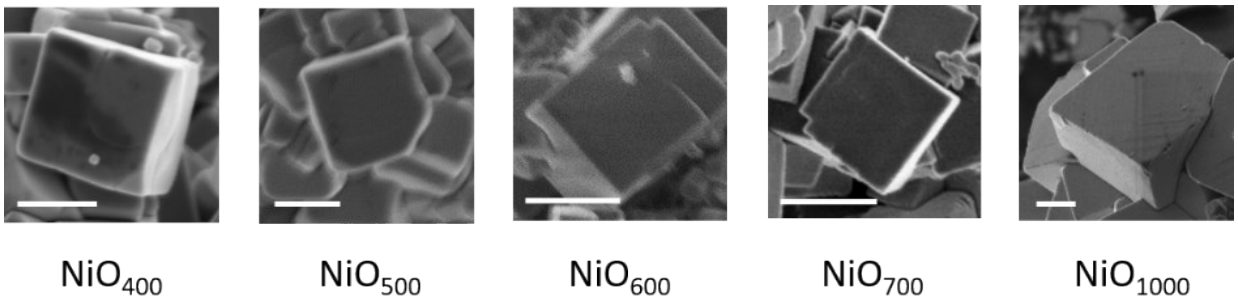

Fig. S3 Scanning electron micrographs of NiO cubes after thermal treatments at 400–1000 °C for 5 h. Scale bars equal 1 μm.

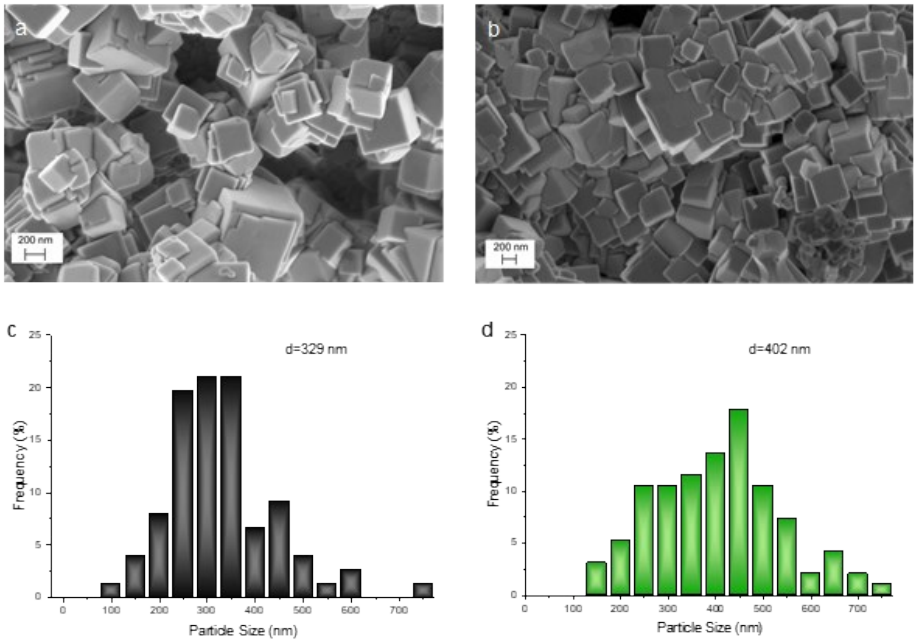

Fig. S4 SEM images of NiO catalysts after thermal treatment at a) 400 ºC and b) 1000 ºC for 5h. Histograms showing the particle size distribution of c) NiO_{400} and d) NiO_{1000}.

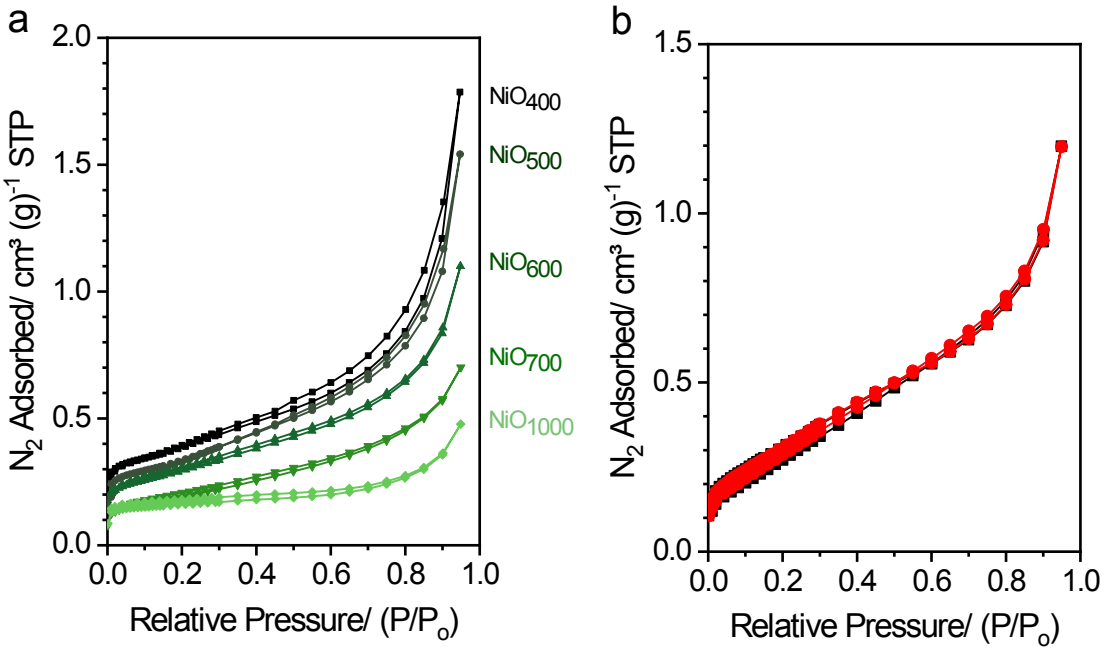

Fig. S5. Nitrogen physisorption isotherms of (a) NiO cubes after thermal treatment at 400–1000 °C for 5 h and (b) Repeat measurments on the NiO_{500} sample.

Table S1 Physical properties of as-synthesized NiO and samples after thermal treatment at 400–1000 °C

sample	S_{BET} (m^2 g^{-1})	TPD onset temperature (°C)	H_2-TPD onset temperature (°C)
NiO as synthesized	1.40	380	-
NiO_{400}	1.33	400	312
NiO_{500}	1.18	428	312
NiO_{600}	0.99	510	325
NiO_{700}	0.77	515	331
NiO_{1000}	0.70	-	351

Table S2 XPS-derived surface atomic compositions of NiO samples thermally treated at 400, 700, and 1000 °C.

Atomic %	NiO_{400}	NiO_{700}	NiO_{1000}
O	44.2	48.2	48.8
Ni	27.6	33.7	37.1
C	27.1	16.4	14.2
Na	1.1	1.4	<0.1
K	<0.1	<0.1	<0.1

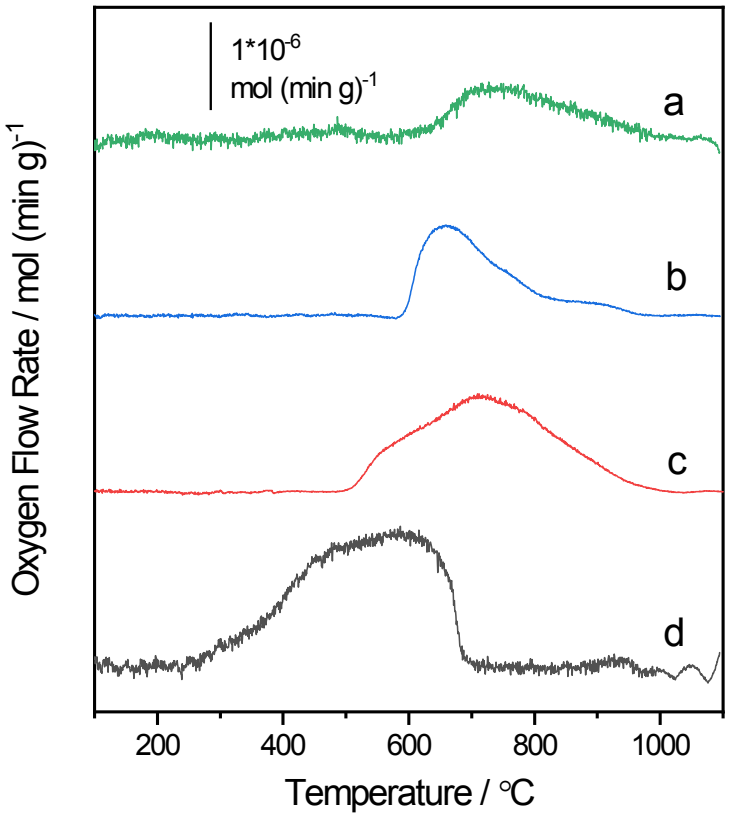

Fig. S6 TPD profiles of as-synthesized $Ni_{1-x}O$ cubes thermally treated under various conditions prior to O_2 desorption analyses as follows: (a) heated up inside the reactor to 600 °C and maintained for 5 h following by natural cooling to room remperature under 100 mL min^{-1} He flow (TPD analysis immediately followed without exposure to air), (b–c) similarly treated in a muffle furnace under static lab air at 600 °C for (b) 0, (c), 5 and (d) 15 h (i.e., exposed to ambient conditions and then transferred to the reactor for TPD measurements). In all cases, heating rates were 2.5 °C min^{-1}.

In Fig. S7, the UV–Vis absorption spectra after TPD (traced green) are shown in comparison with those measured before TPD (traced black). For NiO_{400}–NiO_{700} samples, subjection to TPD protocols increased their degree of stoichiometry, and therefore they showed lower absorption backgrounds. For NiO_{1000}, the absorption spectrum was not altered after TPD, suggesting that the highest degree of stoichiometry has been reached at 1000 °C, and did not increase further upon TPD.

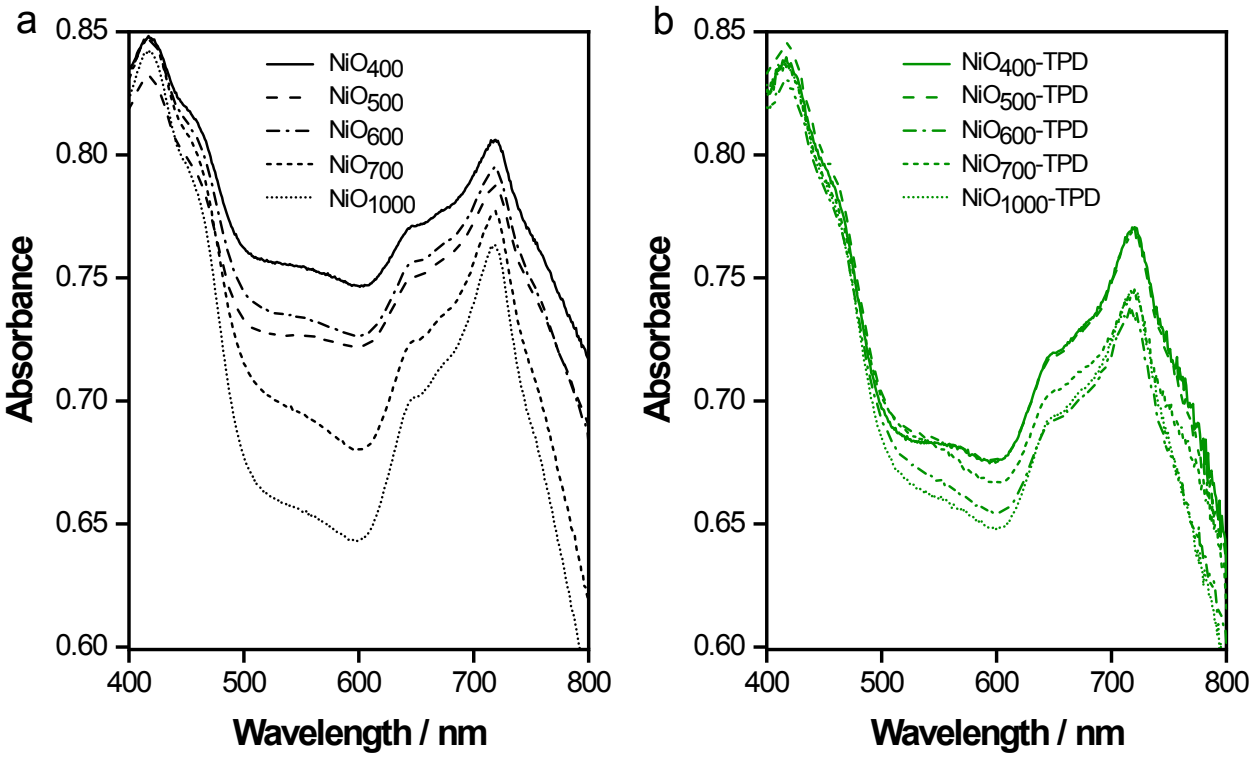

Fig. S7 (a) UV–Vis absorption spectra of NiO cubes thermally treated at different temperatures after synthesis (indicated in the legend), and (b) corresponding absorption spectra of the same samples after TPD meaurements.

2. Kinetic results of ethane ODH over NiO

2.1 *Approach-to-equilibrium.* The approach-to-equilibrium η ($0 \leq \eta \leq 1$) measures the distance of the reaction from equilibrium. Under typical operating conditions for ODHE: 700 K, P_{C2H6} = 10 kPa, P_{O2} = 10 kPa and 10% conversion, the values of η for all three reactions are much smaller than unity (eq. S3, S6, S9), suggesting that the reactions are far from equilibrium with negligible extent of reverse reaction. Therefore, the overall reaction rate $v = v^+ - v^- = v^+$.

$$C_2H_6 + \frac{1}{2}O_2 \rightarrow C_2H_4 + H_2O \qquad \Delta G^0_{700K}\,(ODH) = -180\ kJ/mol \tag{S1}$$

$$K_{eq,\,ODH} = \exp\left(-\frac{\Delta G^0_{700K}}{RT}\right) = 2.7 \times 10^{13} \tag{S2}$$

$$\eta_{ODH} = \frac{1}{K_{eq}} \times \frac{[P_{C2H4}][P_{H2O}]}{[P_{C2H6}][P_{O2}]^{0.5}} = 1 \times 10^{-16} \tag{S3}$$

$$C_2H_6 + \frac{7}{2}O_2 \rightarrow 2CO_2 + 3H_2O \qquad \Delta G^0_{700K}\,(ethane\ total\ oxidation) = -1601\ kJ/mol \tag{S4}$$

$$K_{eq,\,ethane\ total\ oxidation} = \exp\left(-\frac{\Delta G^0_{700K}}{RT}\right) = 3 \times 10^{119} \tag{S5}$$

$$\eta_{ethane\ total\ oxidation} = \frac{1}{K_{eq}} \times \frac{[P_{H2O}]^3[P_{CO2}]^2}{[P_{C2H6}][P_{O2}]^{3.5}} = 5 \times 10^{-123} \tag{S6}$$

$$C_2H_4 + 3O_2 \rightarrow 2CO_2 + 2H_2O \qquad \Delta G^0_{700K}(ethane\ total\ oxidation) = -1388\ kJ/mol \tag{S7}$$

$$K_{eq,\,ethene\ total\ oxidation} = \exp\left(-\frac{\Delta G^0_{700K}}{RT}\right) = 4 \times 10^{103} \tag{S8}$$

$$\eta_{ethene\ total\ oxidation} = \frac{1}{K_{eq}} \times \frac{[P_{H2O}]^2[P_{CO2}]^2}{[P_{C2H4}][P_{O2}]^3} = 1.4 \times 10^{-107} \tag{S9}$$

where $\Delta G^{0}_{700K}(i)$ is the standard Gibbs free energy at 700 K, $K_{eq,i}$ is the equilibrium constant, and η is the approach-to-equilibrium of reaction i.

2.2 *Selectivity-conversion data.* Decreasing ethene selectivity with increasing ethane conversion (Fig. S8) is consistent with the conversion of ethene to CO_2 through secondary reactions (r_3). The existence of r_3 from ethene to CO_2 is also consistent with decreasing ethene formation rates with increasing residence time (Fig. S9). However, CO_2 formation rates were also found to decrease, not increase, with residence time, which is inconsistent with CO_2 formation through secondary reactions; therefore, we suspect that CO_2 formation is inhibited by product concentrations.

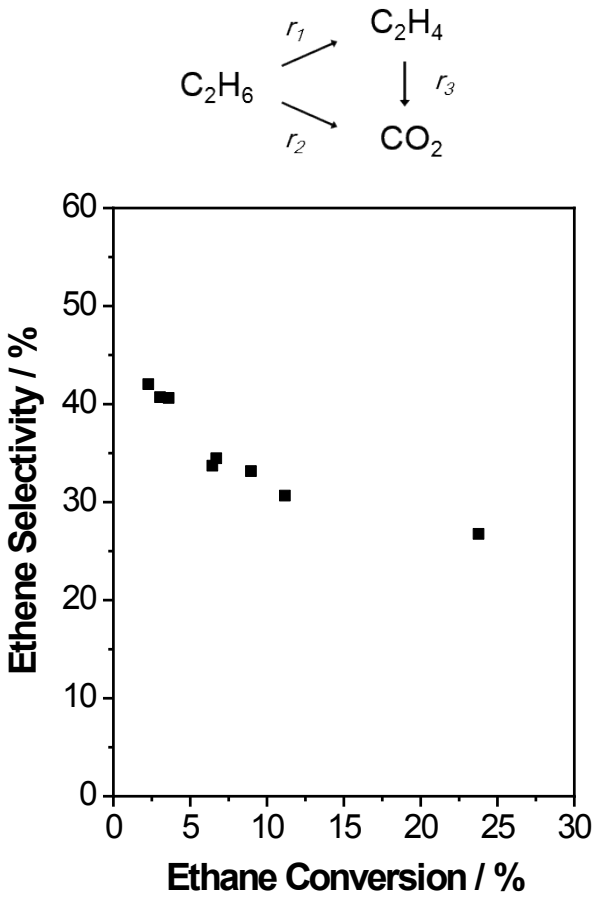

Scheme S2. Proposed reaction network for ethane oxidation reactions

Fig. S8 Ethene selectivity plotted as a function of ethane conversion. Increasing ethane conversion was achieved by increasing residence times from 0.1 to 1.6 g s cm^{-3}. Reaction conditions: 375 °C, 10 kPa C_2H_6, 10 kPa O_2, balance He.

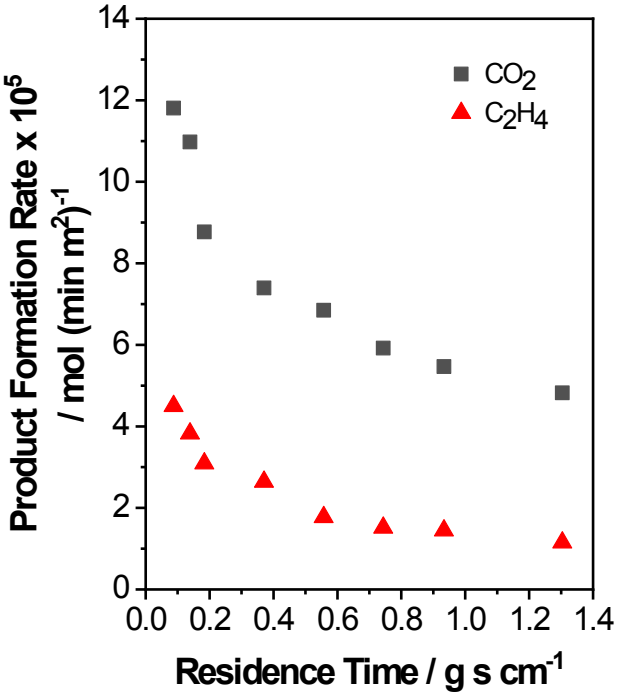

Fig. S9 Formation rates of ethene（▲） and CO_2 (■) as a function of residence time. Reaction conditions: 375 °C, 10 kPa C_2H_6, 10 kPa O_2, balance He.

2.3 *Ethene oxidation.* Rates of ethene oxidation—the secondary reaction of ethane ODH—were tested. CO_2 and H_2O are the only observed products. Ethene showed rates comparable to the total oxidation of ethane (Fig. S10a). Meanwhile, ethene oxidation rates increased with C_2H_4 pressure (Fig. S10b). Based on these results, we expect that with 0.04 kPa C_2H_4 at typical ethane conversions, r_3 was approximately 2.1×10^{-7} mol min^{-1}, w hich was insignificant compared with r_2.

Table S3. Bond dissociation energy (BDE) of ethane (C_2H_6) and ethene (C_2H_4) at 298 K[1]

molecule	bond type	BDE (kJ/ mol)
CH_3CH_3	C-C	368
	C-H	410
$H_2C=CH_2$	C=C	682
	C-H	452

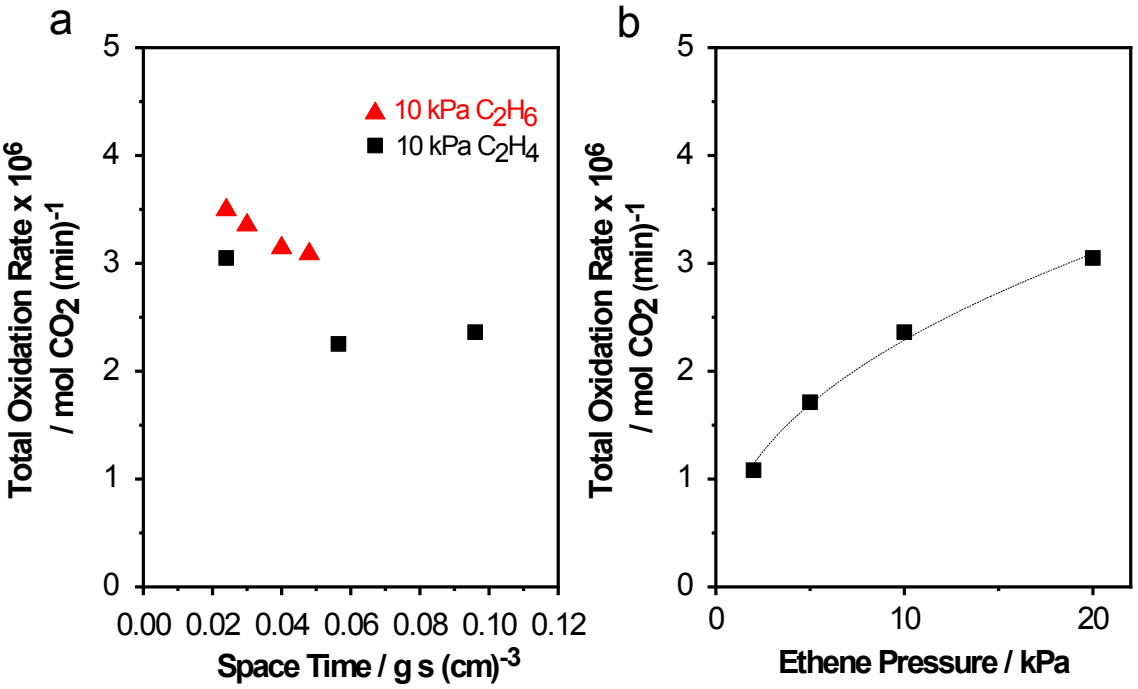

Fig. S10 (a) Total oxidation rate of ethane (▲) and ethene (■).Reaction conditions: 375 °C, 10 kPa C_2H_6/C_2H_4, 10 kPa O_2, balance He. (b) CO_2 formation rate at increasing ethene pressure. Reaction conditions: 375 °C, 10 kPa O_2, 2-20 kPa C_2H_4, balance He.

2.4 *Water inhibition*. Decreasing ethene and CO_2 formation rates with residence time are consistent with the presence of product inhibition. To test this hypothesis, 1–10 kPa H_2O was cofed during reaction. We observed decreasing rates with increasing H_2O pressure; besides, these rates are invariant in residence time, consistent with H_2O inhibition. We envision that in the absence of water cofeeds, the average water pressure increases with conversion (Scheme S2a), thereby exerting a stronger inhibiting effect at higher residence times, which would explain the decreasing ethene and CO_2 formation rates with increasing residence time. Cofeeding excess water during ODHE creates constant water pressures along the bed, resulted in non-integral beds whose rates can directly be calculated from product molar flow rates (Scheme S2b).

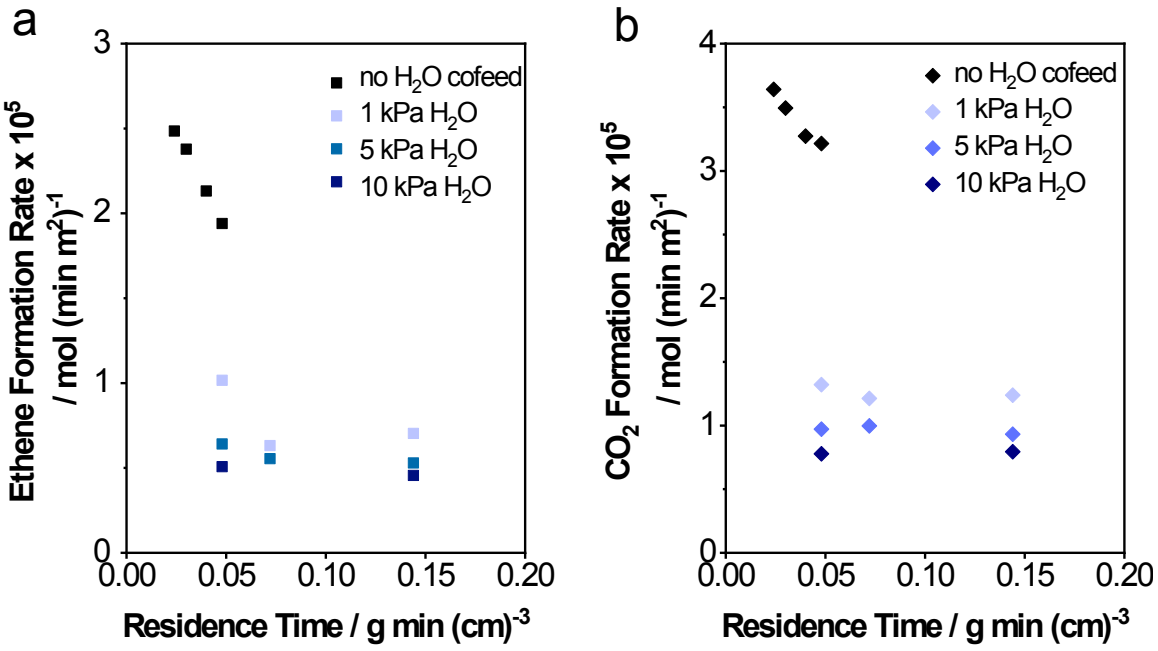

Fig. S11 Water inhibition effect on (a) ethene and (b) CO_2 formation rates. Reaction conditions: 400°C, 10 kPa C_2H_6, 10 kPa O_2, and 1–10 kPa H_2O.

Scheme S2 Diagrams representing reaction rate (a) before and (b) after water cofeeds as a function of residence time.

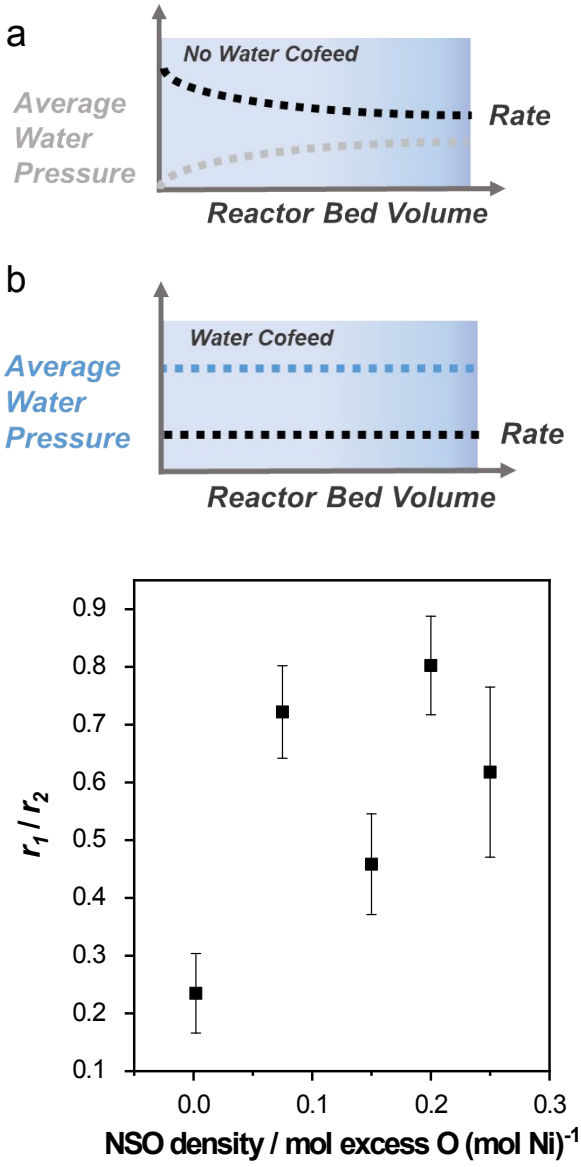

Fig. S12 Ratios of ODHE (r_1) to total oxidation rates (r_2) as a function of TPR-derived NSO density for samples NiO_{400} to NiO_{1000}. Error bars were obtained from rate measurements at three distinct residence times. Reaction conditions: 375 °C, 10 kPa C_2H_6, 10 kPa O_2, 1 kPa H_2O; C_2H_6 conversion less than 1%.

3. Derivation of the formula for TPD and TPR-derived NSO densities

$Ni_{1-x}O$ samples with x being unknown have a molar mass $M_{Ni_{1-x}O} = (1-x) \times 58.7+16$ g mol^{-1}. The total moles of sample, and the moles of Ni and O can then be expressed based on the mass of sample loaded during the TPD experiment (0.25 g). The difference between N_{Ni} and N_O is equal to the total moles of O desorbed during the TPD experiment, hence x can be solved for by integrating molar flow rates of O_2 over time. Once x is calculated, the NSO density can be further obtained.

$$M_O = 16 \left(\frac{g}{mol}\right), M_{Ni} = 58.7 \ (\frac{g}{mol}) \tag{S10}$$

$$M_{Ni_{1-x}O} = (1-x) * 58.7 + 16 \quad (\frac{g}{mol}) \tag{S11}$$

$$N_{Ni_{1-x}O} = N_O = \frac{0.25}{M_{Ni_{1-x}O}} \ (mol) \tag{S12}$$

$$N_{Ni} = \frac{(1-x) * 0.25}{M_{Ni_{1-x}O}} \ (mol) \tag{S13}$$

$$N_O - N_{Ni} = \frac{0.25x}{M_{Ni_{1-x}O}} = \frac{0.25x}{(1-x) * 58.7 + 16} = \frac{N_{O2,\,desorb}}{2} \ (mol) \tag{S14}$$

$$NSO\ density = \frac{x_{TPD}}{1-x_{TPD}} = \frac{74.7\ N_{O2,desorbed}}{0.5 - 16N_{O2,desorbed}} \quad \left(\frac{mol\ excess\ O}{mol\ Ni}\right) \tag{S15}$$

where M_O and M_{Ni} are the atomic mass of oxygen and nickel

x is the degree of non-stoichiometry in $Ni_{1-x}O$

$M_{Ni_{1-x}O}$ is the molar mass of $Ni_{1-x}O$

$N_{Ni_{1-x}O}$, N_O, N_{Ni} are the mole of $Ni_{1-x}O$, O and Ni

$N_{O2,\,desorb}$ is the total mole of O_2 that desorb during TPD

x_{TPD} is the degree of non-stoichiometry of $Ni_{1-x}O$ as determined by TPD

In TPR experiments, the moles of Ni and O can be expressed in the same way based on the mass of sample loaded (0.02 g). The term N_O is equal to the total moles of H_2 consumed during the H_2-

TPR experiment, following $Ni_{1-x}O + H_2 \rightarrow (1-x_{TPR})\ Ni + H_2O$. Therefore, x can be solved by calculating the total moles of H_2 consumed over time.

$$N_{Ni_{1-x}O} = N_O = \frac{0.02}{M_{Ni_{1-x}O}} = \frac{0.02}{(1-x)*58.7+16} = N_{H2,\ consumed} \quad (mol)$$

(S16)

$$NSO\ density = \frac{x_{TPR}}{1-x_{TPR}} = \frac{74.7\ N_{H2,consumed} - 0.02}{0.02 - 16 N_{H2,consumed}} \quad \left(\frac{mol\ excess\ O}{mol\ Ni}\right)$$

(S17)

where $N_{H2,\ consumed}$ is the total moles of H_2 that consumed during H_2-TPR

x_{TPR} is the degree of non-stoichiometry of $Ni_{1-x}O$ as determined by H_2-TPR

References

1 H. Schobert, in *Chemistry of Fossil Fuels and Biofuels*, Cambridge University Press, 2013.